# Analysis of LVE behaviour and fatigue damage evolution of asphalt pavements with different interface conditions in an accelerated full-scale experiment

X Q Le, Mai Lan Nguyen, Pierre Hornych, Q T Nguyen

▶ **To cite this version:**

X Q Le, Mai Lan Nguyen, Pierre Hornych, Q T Nguyen. Analysis of LVE behaviour and fatigue damage evolution of asphalt pavements with different interface conditions in an accelerated full-scale experiment. International Journal of Pavement Engineering, 2022, pp.1-14. 10.1080/10298436.2022.2147522 . hal-04313081

**HAL Id: hal-04313081**

**https://univ-eiffel.hal.science/hal-04313081**

Submitted on 28 Nov 2023

**HAL** is a multi-disciplinary open access archive for the deposit and dissemination of scientific research documents, whether they are published or not. The documents may come from teaching and research institutions in France or abroad, or from public or private research centers.

L'archive ouverte pluridisciplinaire **HAL**, est destinée au dépôt et à la diffusion de documents scientifiques de niveau recherche, publiés ou non, émanant des établissements d'enseignement et de recherche français ou étrangers, des laboratoires publics ou privés.

Distributed under a Creative Commons Attribution - NonCommercial - NoDerivatives 4.0 International License

# Analysis of LVE behavior and fatigue damage evolution of asphalt pavements with different interface conditions in an accelerated full-scale experiment

X.Q. Le[a,b], M.L. Nguyen[a*], P. Hornych[a], Q.T. Nguyen[b]

[a] *MAST-LAMES, Gustave Eiffel University, Nantes, France;* [b] *University of Transport and Communications, Hanoi, Vietnam*

*corresponding author: mai-lan.nguyen@univ-eiffel.fr

Total word count of the manuscript: 9185

# Analysis of linear viscoelastic behavior and fatigue damage evolution of asphalt pavement layers with different interface conditions in an accelerated full-scale experiment

For better optimization of pavement design and management processes, great efforts have been made to interpret the fatigue behavior of pavements during their service life. Among interesting methods, accelerated full-scale pavement tests (APT) represent very efficient tools to study pavement behavior from initial to damaged condition. This paper presents an experimental study where three asphalt pavements with different interface conditions between the asphalt layers were tested in an APT experiment. An original methodology was proposed to assess pavement behavior with such different interface conditions. Asphalt layer strains, Falling Weight Deflectormeter (FWD) deflections, and surface cracking of the pavements were monitored during the experiment. First, strain signals and pavement surface deflections measured at the beginning of the experiment, when the pavement was not damaged, were used to characterize the viscoelastic properties of the asphalt layers, based on an original measurement and calibration procedure applied at different traffic speeds. Then the different measurements were used to analyze the fatigue behavior of the experimental pavements, and the evolution of their level of damage to traffic. The analysis showed that in such asphalt pavements having different interface conditions, asphalt layer strains, which varied significantly with the increase of load cycles due to their dependency on both local crack development around the strain gauges and on the asphalt layers interface conditions, were not suitable for estimating an “average” asphalt layer damage. In order to monitor the general pavement behavior, a new damage ratio was introduced based on FWD backcalculated moduli of the asphalt layers. The proposed indicator allowed to observe a stiffness increase of the asphalt layers at the beginning of the loading application due to aging and post compaction, and then fatigue damage was the main cause of the pavement behavior evolution which had a very good correspondence with surface cracking.

Keywords: accelerated full-scale test; asphalt pavement; linear viscoelastic behavior; fatigue damage; interface condition

## 1. Introduction

Understanding pavement damage mechanisms and their evolution during pavement service life are essential for the development of pavement design and management methods. Several methods have been developed to assess pavement properties at different levels, from laboratory testing on material samples, through real scale structure and road section up to pavement network. Among those, full-scale accelerated pavement tests (APT) where pavements can be tested under controlled loading conditions up to failure in a short period represent very efficient tools to study pavement performance (Autret et al., 1987; Blanc et al., 2019; Mateos et al., 2012; Nguyen et al., 2020a).

For studies on asphalt pavement structures, linear viscoelastic properties of asphalt materials characterized in laboratory, have usually been used in numerical modeling to simulate pavement responses and to compare with experimental measurements using embedded sensors or falling weight deflectometer (FWD) tests among other procedures. However, few studies have been done to characterize the linear viscoelastic properties of asphalt layers by direct measurements on pavement structures. Recent studies have shown that analyzing material properties at the structural level is not evident, due to the influence of interface conditions between the asphalt layers on the response of the pavement structure.

In this study, an accelerated full-scale fatigue experiment (Figure 1) was carried out at Gustave Eiffel University, in Nantes campus, on three pavement sections with the same structure, consisting of two asphalt layers. The first section was a reference structure, consisting of two standard layers of asphalt concrete with a normal average tack coat application rate. The two other structures were reinforced with two different fiberglass grids, placed at the interface between the two asphalt layers using a double rate

of the same tack coat. The objective of the study was to evaluate the mechanical behavior of the pavement structures having such different interface conditions throughout the experiment, from initial to damaged condition. In this work, different types of measurements including strain gauge measurements, FWD tests, and surface cracking surveys have been performed all along with the experiment and allowed to evaluate the linear viscoelastic behavior of the asphalt layers in each pavement section under non-damaged condition and the evolution of their damage with the number of load cycles. The response of the pavement structures was then compared with predictions obtained by modeling based on laboratory material properties.

Figure 1. Full-scale accelerated fatigue experiment on asphalt pavements at Gustave Eiffel University in Nantes.

The paper presents first the tested pavement structures and the experimental program. The mechanical response of the undamaged pavement structures is then evaluated, based on strain measurements at the bottom of the asphalt layers, under different loading conditions. These measurements in the asphalt layers are used together with FWD backcalculated moduli of the other pavement layers to characterize the viscoelastic behavior of the asphalt layers at different traffic speeds, and make comparisons with complex modulus values measured on asphalt samples in the laboratory. Finally, the evolution of pavement fatigue damage with traffic is evaluated

based on the analysis of strain response, surface cracking and back-calculated pavement layer moduli.

## 2. Pavement structures, materials and monitoring methods

### *2.1. Pavement structures and materials*

#### *2.1.1. Pavement structures*

Three different pavement sections (denoted A, B, and C – see Figure 2) were tested in the experiment. Section A has a traditional asphalt pavement structure with two asphalt layers made with the same mix and is considered as the reference section. The design thicknesses of these layers are 6 cm and 5 cm for the surface and base layers respectively. These asphalt layers were laid on a 30 cm thick unbound granular material (UGM) subbase and a subgrade consisting of silty sand, about 260 cm thick, all built above a concrete slab, present at the bottom of the APT track. Sections B and C have the same structure and materials as in section A, but have each an interlayer system made of a glass fiber grid of different types (grid G5 with a tensile strength of 100 kN/m and grid G1 with a tensile strength of 50 kN/m, respectively) at the interface of the two asphalt layers.Both grids, coated with styrene butadiene rubber (SBR) resin, have the same mesh size of 40 mm × 40 mm and are associated with a thin non-woven polyester layer of 17 g/m².

The actual total thicknesses of the asphalt layers in sections A, B and C, measured every meter along the test track, using leveling measurements made during construction, gave average thicknesses of 11.4, 10.3, and 10.3 cm respectively. These measurements show that the reference section A has the thickest asphalt layer, whereas the two sections B and C with grid have similar asphalt thicknesses, about 1.1 cm lower than the reference section.

The same tack coat consisting of a classical cationic rapid setting bitumen emulsion (according to standard EN 13808 (2013)) was applied at the asphalt layers interface with rates of 350 g/m² and 700 g/m² (in residual bitumen) for sections without and with grid respectively. It is noted that the latest tack coat rate was chosen, based on an extensive laboratory study (Godard et al., 201) carried out on specimens with different application rates, as the one that gave the best performance for both types of grid. Hence, the three tested pavement sections presented different conditions at the interface between the asphalt layers. First evaluations of these interface conditions were made in laboratory using direct tension bonding tests conducted on double-layered cylindrical specimens extracted from the full-scale pavement sections before loading and on control material specimens fabricated in laboratory with the same configurations. The results, presented in recent studies (Godard et al., 2019; Le et al., 2022), showed that the specimens with 100 kN and 50 kN grids had average values of interface tensile strength about three times (0.22 MPa) and two times (0.39 MPa) lower than the reference specimens without grid (0.77 MPa).

Each pavement section was divided in two subsections (1 and 2; each about 10 m long and 3 m wide) (Figure 2):

- Subsections 1 (A1, B1, C1) were instrumented with strain gauges, installed at the bottom of each of the two asphalt layers.

- Subsections 2 (A2, B2, C2) were left as “control zones” without instrumentation.

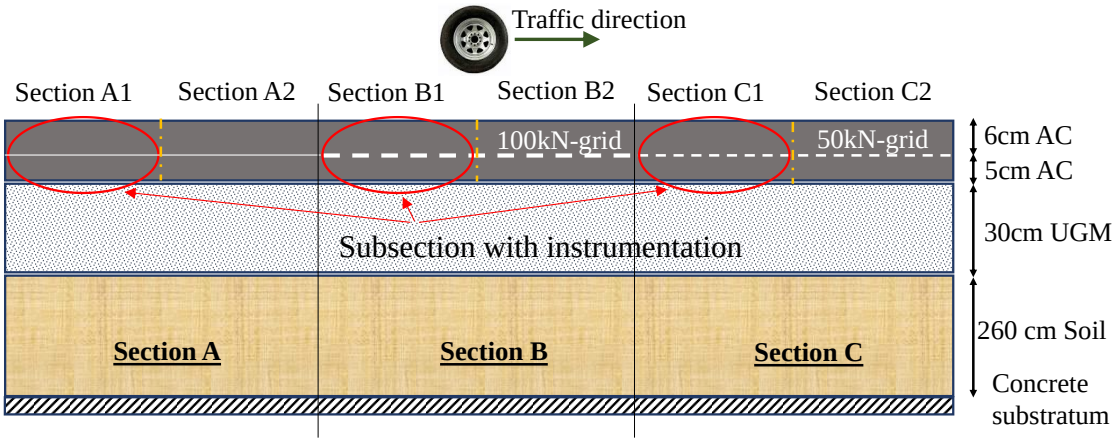


Figure 2. Schematic view of the three tested pavement sections.

### *2.1.2. Asphalt materials*

The design of the asphalt concrete and its main mechanical properties in terms of complex modulus and fatigue behavior are detailed in this section.

*Asphalt concrete design*

The two asphalt layers consist of the same material which is a 0/10mm semi-coarse asphalt concrete (SCAC) of class 3 (according to standard NF EN 13108-1 (2007)). The binder used is a neat bitumen of 35/50 penetration grade (according to EN 12591 (2009) standard), with an average binder content of 5.58 % by mass of aggregates. The gradation of the asphalt mixture is shown in Figure 3.

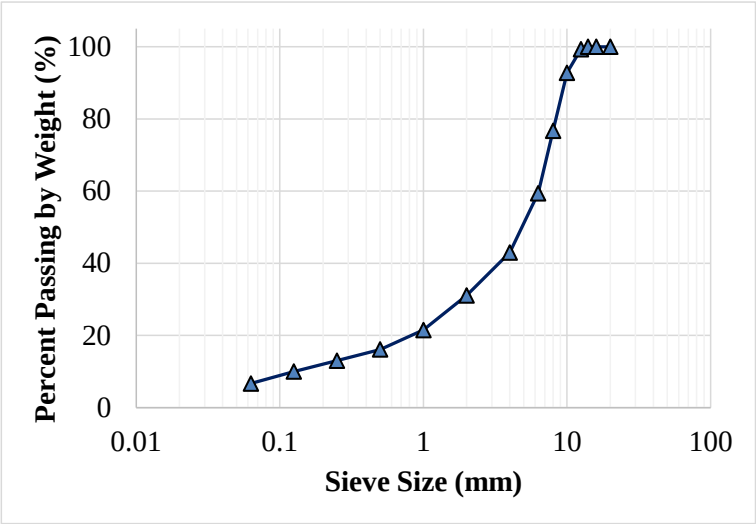


Figure 3. Aggregate grading curve of the asphalt mixture.

*Linear viscoelastic behavior of the asphalt concrete*

The linear viscoelastic (LVE) behavior of the asphalt mix was characterized using Two-Point Bending (2PB) complex modulus tests on trapezoidal specimens, according to standard EN 12697-26 (2018). The tests were performed at six different temperatures (from -10°C to 30°C) and five different frequencies (from 3 Hz to 40 Hz). The tested samples were produced from the field mixture, collected during pavement construction.

Figure 4 presents the isotherms of the norm of the complex modulus of the asphalt mixture measured for each tested temperature, as a function of the loading frequency. From these experimental measurements, a unique master curve was built by applying the time-temperature superposition principle (TTSP), by shifting along the frequency axis the isotherm curves at different temperatures to a reference temperature ($T_{ref}$) of 15°C.

Then, the Huet-Sayegh rheological model (Huet, 1963; Sayegh, 1967) was applied to model the LVE behavior of the tested asphalt mix, based on the complex modulus ($E^*$) results. The expression of $E^*$ according to this model is given in Equation

(1). Others models such as Witczak (Bari & Witczak, 2006), CAM (Marasteanu & Anderson, 1999), or 2S2P1D (Olard & Di Benedetto, 2003) can be used for this modeling. However the Huet-Sayegh model was used in this work, as it will be used in the next step for the linear viscoelastic modeling of the pavement response under moving wheel loads. On Figure 4, it can be seen that the Huet-Sayegh model fits very well the experimental master curve.

$$E^*(i\omega\tau) = E_0 + \frac{E_\infty - E_0}{1+\delta(i\omega\tau)^{-k}+(i\omega\tau)^{-h}} \quad (1)$$

where:

$i$ = imaginary unit,

$\omega$ = frequency in radians per second,

$E_0$ = static modulus when $\omega\tau \rightarrow 0$,

$E_\infty$ = glassy modulus when $\omega\tau \rightarrow \infty$,

$\delta$ = dimensionless calibration constant,

$k = E_{imag}/E_{real}$ ratio when $\omega \rightarrow 0$,

$h = E_{imag}/E_{real}$ ratio when $\omega \rightarrow \infty$,

$\tau$ = characteristic time, expressed as a function of the temperature ($T$) by Equation (2):

$$\tau = e^{(A_0+A_1T+A_2T^2)} \quad (2)$$

The model parameters ($E_0, E_\infty, k, h, \delta, A_0, A_1, A_2$) were determined using the ViscoAnalyse software (Chailleux et al., 2006), and are given in Table 1. These parameters will be used for the modeling of strain signals in section 3.3.

Table 1. Huet-Sayegh's model parameters obtained for the studied asphalt concrete mix.

| Material | $E_0$ (MPa) | $E_\infty$ (MPa) | $k$ | $h$ | $\delta$ | $A_0$ | $A_1$ | $A_2$ |
|---|---|---|---|---|---|---|---|---|
| Asphalt concrete 0/10 | 19 | 27007 | 0.193 | 0.588 | 1.695 | 3.883 | -0.431 | 0.002758 |

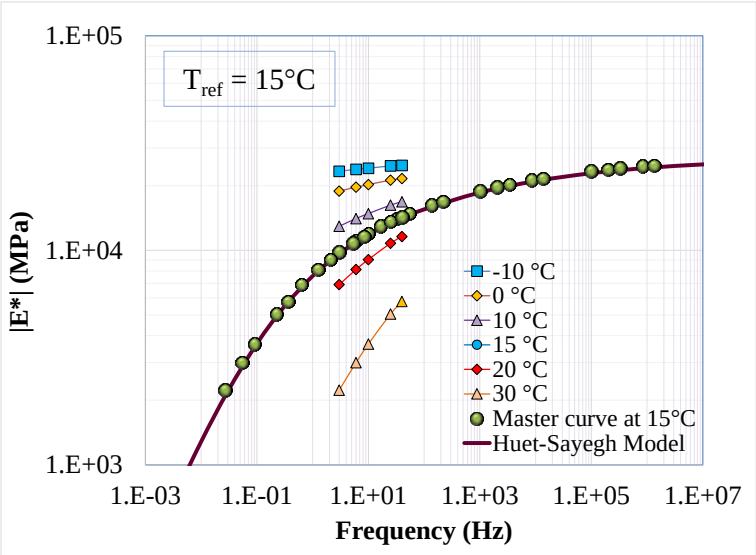


Figure 4. Isotherm curves of $|E^*|$, master curve and fitting with the Huet-Sayegh model, at the reference temperature $T_{ref}$ = 15°C of the studied asphalt concrete mix.

*Fatigue performance*

Fatigue is one of the most important criteria for asphalt concrete performance. In this study, 2PB fatigue tests were performed, according to standard NF EN 13108–1 (2007), to determine the fatigue resistance of the studied asphalt mix. The results of the fatigue tests were used to determine the design parameters (

Table 2), needed for pavement design in accordance with the French Rational Pavement Design Method (RPDM) (NF P98-086 (2019)). Those parameters consist of:

- $\varepsilon_6$: strain, leading to failure for 1 million load cycles.
- *b*: slope of the material fatigue law, expressed in the form of a bi-logarithmic law.
- *SN*: standard deviation on the logarithm of the number of cycles leading to fatigue.

Table 2. Fatigue parameters of the studied asphalt concrete.

| $\varepsilon_6$ min (μm/m) | $\varepsilon_6$ mean (μm/m) | $\varepsilon_6$ max (μm/m) | Fatigue slope *-1/b* | Standard deviation *SN* |
|---|---|---|---|---|
| 110.0 | 114.5 | 118.0 | 6.2 | 0.2 |

### *2.2. Description of the full-scale fatigue experiment*

The three pavement sections were constructed at the radius of 19 m on the circular test track of the APT, and tested until significant fatigue damage was obtained. During the experiment (see the schedule in Figure 5), the fatigue carousel was used to apply traffic loading on the experimental pavement sections. The arms of the fatigue carousel were equipped with standard dual wheels. The tires used were Michelin X Multiway 3D XZE 315/80 R 22.5 inflated with an average pressure of 8.5 bar. During the fatigue loading, a lateral wander of ±52 cm was applied to reproduce the effect of real traffic. Three following loading phases were conducted:

- The first phase was carried out from the 28$^{th}$ of May to 13$^{th}$ of June 2018, with approximately 50 000 equivalent 65 kN dual-wheel loads, as calculated by Equation (3). In this phase, different traffic speeds (between 1 and 12 rounds/min, which corresponds approximately to between 7 and 86 km/h respectively) and three load levels of 45, 55, and 65 kN were applied. The average temperature at the middle of the asphalt layers in this phase was around 25°C.
- The second phase was carried out from the 12$^{th}$ of September 2018 to 22$^{nd}$ of December 2018, with 65 kN dual wheel loads, and most of the time a speed of 57 km/h. This phase was the main fatigue loading phase. The average asphalt temperature in this phase was around 12°C. A total of 1.5 million 65 kN dual wheel loads were applied during this phase.

- The third phase was performed from 9th of January to 8th February 2019. In this phase, 0.35 million additional dual-wheel loads were applied, with a load increased to 75 kN, to accelerate fatigue damage. The average asphalt temperature in this phase was around 7°C.

$$NE(P_{65}) = N(P_i)\left(\frac{P_i}{P_{65}}\right)^{-1/b} \quad (3)$$

Where:

$NE(P_{65})$: Number of equivalent load cycles ($P_{65}$ = 65 kN),

$N(P_i)$: Number of cycles loaded at i kN ($P_i$ = 45, 55, 65, or 75 kN),

b: Fatigue slope of the asphalt material in the Wöhler bi-logarithmic diagram.

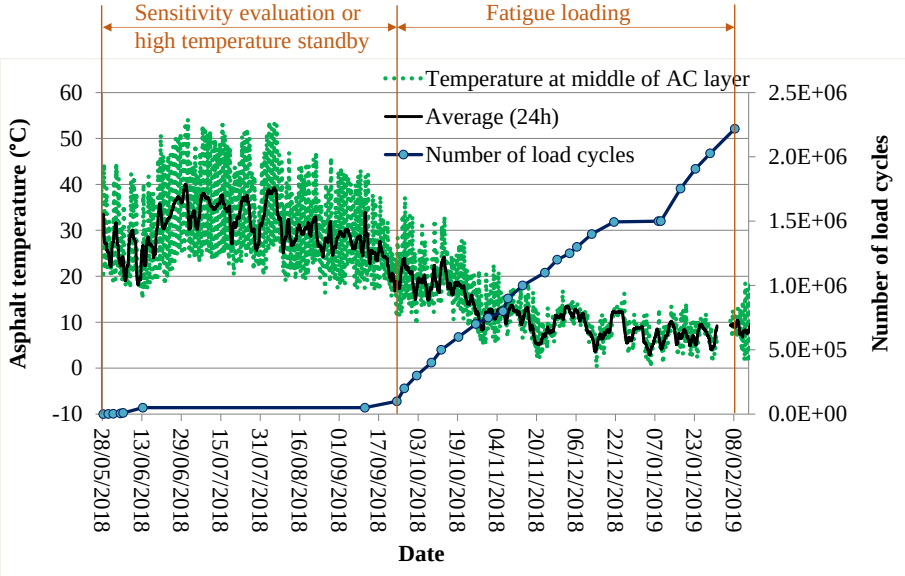


Figure 5. Full-scale fatigue experiment schedule and asphalt temperature data measured at the middle of the asphalt layers.

### *2.3. Monitoring methods*

During the full-scale fatigue experiment, pavement performance was monitored by different measurements carried out with the increase of traffic, including: embedded instrumentation using strain gauges, FWD tests, and surface crack monitoring.

#### *2.3.1. Instrumentation*

Strain gauges (TML type, model KM-100A) were installed, in subsections A1, B1, and C1 as previously mentioned in section 2.1.1 (Figure 2), at the bottom of the surface layer (except on section C1) and at the bottom of the base asphalt layer, during the construction.

Four thermocouple probes were embedded at four different depths (0, 6, 9 and 30 cm) in the pavement structure, in section C, to monitor pavement temperatures. Temperatures were recorded continuously during the experiment, every 10 minutes. The temperatures measured by the probe placed at -6 cm, i.e. at the middle of the asphalt layers, are presented in Figure 5. They are considered as representative of average temperatures in the asphalt layers and are used for further evaluations in this paper. The average asphalt temperatures during loading application were between 7 and 25°C, giving an equivalent temperature determined by the French RPDM of approximately 12°C; In this method, the equivalent temperature is defined as the constant temperature leading to the same fatigue damage as the real temperature variations.

#### *2.3.2. FWD measurements*

To observe the evolution of pavement layer moduli during the full-scale experiment, a series of FWD campaigns were performed, before the start of loading, and after 0.5, 0.75, 1.0, and 2.2 million cycles (Table 3).

Table 3. FWD campaign schedule during the full-scale experiment.

| Series | Number of cycles | Force (kN) | Temperature at the middle of the asphalt layers (°C) |
|---|---|---|---|
| 1 | 0 | 65 | 15 |
| 2 | 500 000 | 65 | 19 |
| 3 | 750 000 | 65 | 14 |
| 4 | 1 000 000 | 65 | 12 |
| 5 | 2 200 000 | 65 | 14 |

Deflection basins were measured using a set of nine geophones, located at different distances from the loading plate of the FWD, and used to backcalculate pavement layer moduli. Back-calculations were performed using the ALIZE-LCPC French pavement design software, which was developed based on the multi-layer linear elastic model of Burmister (1943). In the back-calculation process, iterative computations were made to match the measured deflection basin to the calculated one, using assumed layer moduli. It is underlined that the actual thickness values of the asphalt layers were taken into account in the back-calculation, to obtain results that are more precise than using the nominal thickness values. In addition, a unique layer was considered for the total thickness of the two asphalt layers, meaning a fully bonded assumption at their interface for all three studied pavement sections. It is noteworthy to recall that the back-calculated modulus of the asphalt layer is an apparent value, representing field conditions, with the above assumptions.

### *2.3.3. Monitoring of surface cracking*

During the full-scale test, cracks appearing on the pavement surface were monitored using the crack mapping process described by (Nguyen et al., 2020b). After each loading period, images of the pavement surface were taken continuously along the experimental test track, at intervals depending on the moving speed of the traffic simulator. A crack

map, representing an overview of visible cracks on each pavement section can then be rapidly created using an ad hoc image processing tool, developed for this process. The length of cracks was then evaluated to determine a percentage of cracking, defined as the ratio between the pavement section length affected by visible cracks and its total length.

## 3. Pavement response in non-damaged condition

In this section, the mechanical behavior of the tested pavements in non-damaged condition (at the beginning of the experiment) is analyzed, based on strain signals measured at the bottom of the base asphalt layer at the beginning of traffic loading. The focus is made on evaluating experimentally the relationship between geometrical characteristics of the strain signals in the time domain and the corresponding loading speeds. Together with the analysis of the effects of asphalt temperatures and load levels on strain responses, as well as the modeling of the measured strain signals, an original procedure is proposed for the determination of the asphalt layer stiffness in each studied pavement section.

### *3.1. Strain responses at different traffic speeds*

According to previous studies (Hornych et al., 2008; Nguyen et al., 2020a; Timm & Priest, 2008), for similar pavement structures with thick asphalt layers and for dual-wheel loads in single half axle configuration, longitudinal strains are higher than transverse strains and lead to transversal cracks. For this reason, in this study, pavement responses and fatigue damage evolution will be analyzed based on longitudinal strain measurements. Figure 6a presents a typical longitudinal strain signal at the bottom of the base layer of the pavement structure, in the time domain. This signal presents one extension peak ($A_{max}$) and two (pre and post) contraction peaks ($A_{min1}$ and $A_{min2}$). As shown on the figure, it is possible to estimate the period (or loading time) of the signal

either based on the time interval between the two peaks in contraction ($A_{min1}$ and $A_{min2}$), or between the two points where the strain signal passes by zero ($t_{01}$ and $t_{02}$); the corresponding time intervals are respectively denoted as $\Delta t_{min}$ and $\Delta t_0$.

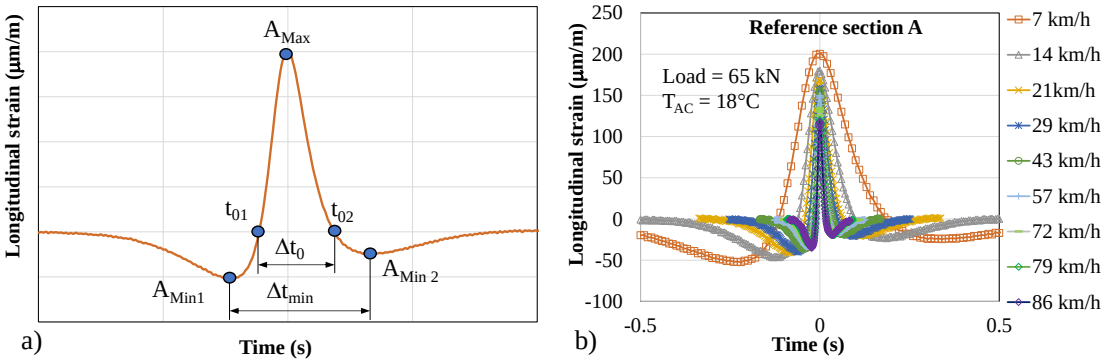


Figure 6. a) Representation of a longitudinal strain signal, with its geometrical characteristics, in the time domain; b) Measured longitudinal strain signals at the bottom of the base layer, in the reference section, at different traffic speeds, at about 8 400 load cycles.

To characterize the evolution of the pavement response with traffic speed, in the non-damaged state, longitudinal strain signals measured at the bottom of the base asphalt layer, in the reference section, at different speeds, are plotted in Figure 6b. These measurements were carried out at an asphalt temperature of 18°C and at about 8 400 load cycles, where it is assumed that the pavements presented no damage. It can be seen that the measured maximum tensile strain, as well as the two loading time parameters ($\Delta t_{min}$ and $\Delta t_{0)}$ of each strain signal vary with traffic speed.

Figure 7 presents the evolution of the strain signal parameters with traffic speed, for all three studied pavement sections A, B and C. These figures show that at low speed (< 30 km/h), the three parameters $A_{max}$, $\Delta t_{min}$ and $\Delta t_0$ decrease rapidly with traffic speed. At higher speeds, the variation is less important. This results from the viscoelastic behavior of asphalt mixes, and similar results can be found in the literature (Bodin et al.,

2017; Brown, 1973; Mshali & Steyn, 2020; Swett et al., 2008; Ulloa et al., 2013). Generally, for a traditional asphalt pavement at a given temperature and asphalt thickness, the decrease of maximum tensile strains and loading times with traffic speed can be described using natural logarithmic functions. Based on the actual experimental data in the present work, negative exponential functions were found to give similar predictions for the maximum strains and even better fits for the two loading time parameters. From the results obtained using these last fitting functions, as presented in these figures, it can be seen that the maximum tensile strains corresponding to the two highest traffic speeds present some difference with the fitting curves, whereas the loading time parameters are all well predicted by the exponential functions.

Considering that the loading times ($\Delta t_{min}$ and $\Delta t_0$) determined previously correspond respectively to the periods of one sinusoidal loading cycle (for $\Delta t_{min}$), and one-half of a loading cycle (for $\Delta t_0$ ), it is possible to determine the corresponding "equivalent frequency" of a sinusoidal load signal, similar to the loading frequency used in laboratory complex modulus tests. For $\Delta t_0$, this assumption is similar to the one defined in (Barksdale, 1971) and mentioned in (Brown, 1973). Hence, the corresponding frequencies can be calculated as follows:

$$f(\Delta t_{min}) = \frac{1}{\Delta t_{min}} \quad (4)$$

$$f(\Delta t_0) = \frac{1}{2\Delta t_0} \quad (5)$$

Figure 7b, 7d and 7f present the calculated "equivalent frequencies" as a function of $\Delta t_{min}$ and $\Delta t_0$ obtained for sections A, B and C respectively. The two obtained frequencies, $f(\Delta t_{min})$ and $f(\Delta t_0)$, are very similar, and present a linear variation with traffic

speed. This experimental finding confirms the results of numerical parametric studies made by (Bodin et al., 2017) and (Ulloa et al., 2013) and some other mathematical linear relationships proposed in the literature (Austroad, 2012; Franken, 1997). Among the two determined frequencies, the slope of the linear function for $f(\Delta t_0)$ seems to vary less for the three pavement sections in this study. This can probably be explained by the fact that $\Delta t_0$ (which considers only the part in extension of the strain signal) is less affected by the difference in layers interface condition between different pavement sections than $\Delta t_{min}$ (which considers both parts in extension and in contraction). $f(\Delta t_0)$ will be used for further analyses in the paper.

It is underlined that the results presented here apply to pavement structures with only one asphalt layer thickness (about 11 cm) and to a limited range of asphalt temperatures (between 18 and 28°C, see Figure 5) corresponding to actual weather conditions recorded at the beginning of the experiment. It would be interesting to extend this analysis to other pavements structures, with different asphalt thicknesses, and to a larger temperature range.

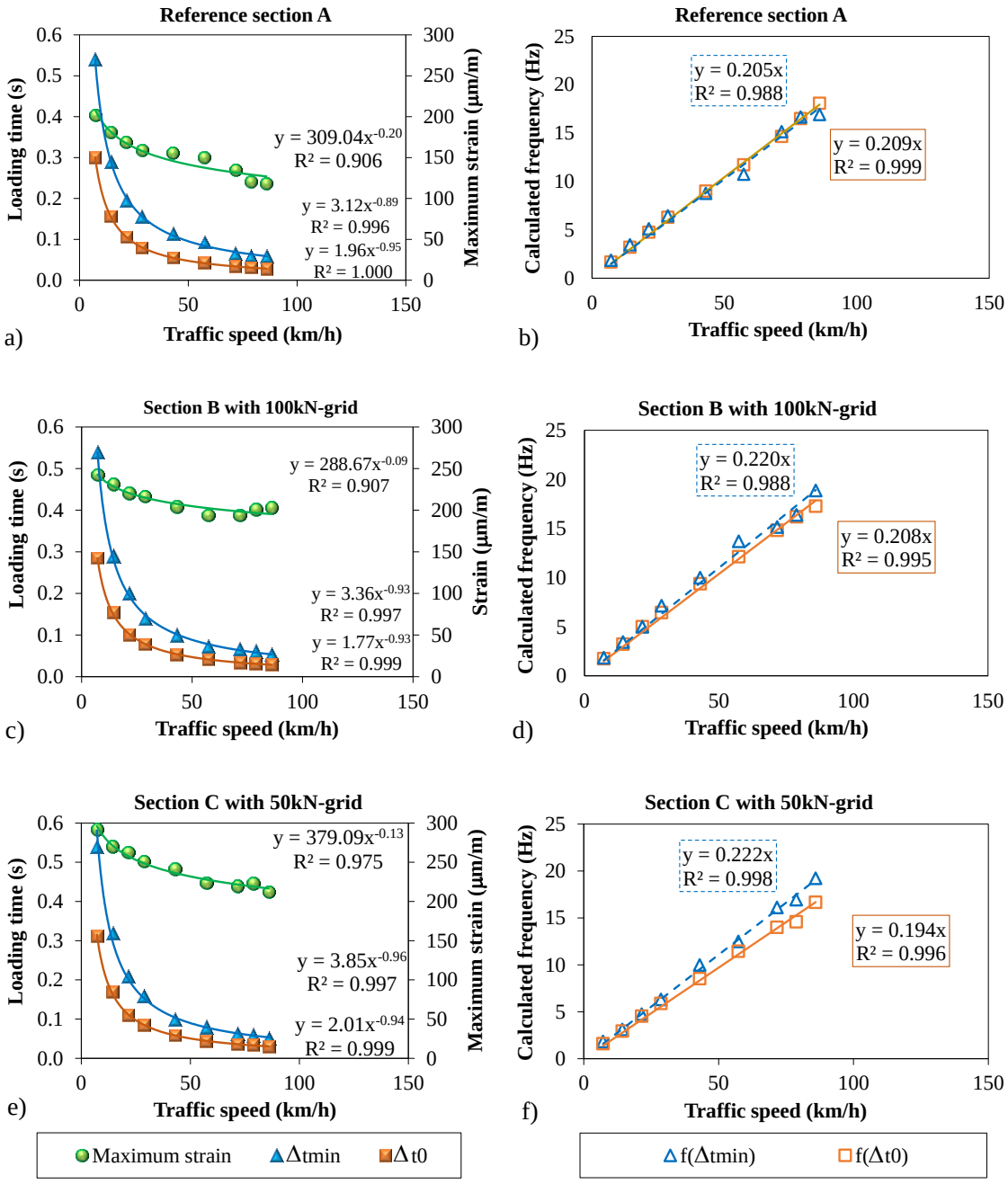


Figure 7. Evolutions of maximum strain, $\Delta t_{min}$ and $\Delta t_0$ (a, c, e) and equivalent loading frequencies calculated with $\Delta t_{min}$ and $\Delta t_0$ (b, d, f) with traffic speed. Results at 8 400 cycles, 65 kN load and a temperature of 18°C.

### *3.2. Effects of load level and temperature*

This section examines the effects of applied load level and of temperature on the equivalent traffic frequency.

Figure 8a presents equivalent frequencies calculated for the reference section A, for three different load levels (45, 55 and 65 kN), and for a similar asphalt temperature (around 21°C). It shows that the equivalent frequencies were not affected by load level for the load range above. Almost the same slope of 0.21 is obtained for the three frequency/speed relationships. Similar results, with slightly different linear relationships, were also obtained for pavements sections B and C, but are not presented here, for lack of space.

According to previous work based on numerical simulations or experimentations found in the literature (Bodin et al., 2017; Willis et al., 2009), the effect of temperature on asphalt pavement response is more important than the effect of traffic speed. Figure 8b presents equivalent frequencies $f(\Delta t_0)$, as a function of traffic speed obtained for section A, for three different asphalt temperatures. It can be seen that the slope of the linear relationship (and thus of the equivalent frequency) increases with temperature in the evaluated asphalt temperature range (between 18 and 28°C). This analysis can be extended in future APT experiments with experimental measurements carried out at a wider range of temperatures.

The established speed–loading frequency relationships depend on temperature, but not on the applied load level, which means that they could be applied for numerical modeling at different temperatures, regardless of the load level.

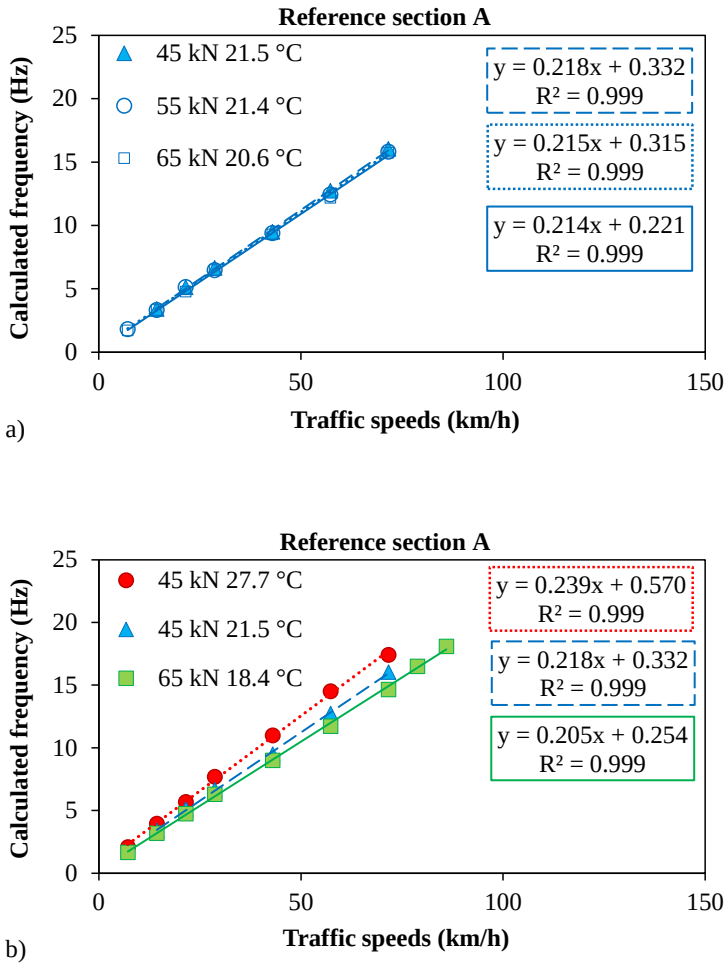


Figure 8. Evolutions of "equivalent" frequency with traffic speed for reference section A during the first 8 400 cycles: a) under three different load levels and at a similar temperature; b) at three different asphalt temperatures.

### *3.3. Modeling of strain signals*

This section presents the modeling of strain signals measured at the bottom of the asphalt layers in the three studied pavement sections, and comparisons with measurements. As an example, modeling was carried out for measurements made at about 8 400 load cycles, under a load level of 65 kN, a speed of 57 km/h, and a temperature of 18.4°C.

In this paper, the modeling is carried out considering the two asphalt layers of the structure as a single layer, and neglecting the interface, and also the grid present in

sections B and C. The considered stiffness (or apparent modulus) is thus an average value representative of all the asphalt layers.

For the modeling, two models were successively applied:

- First, calculations were performed with a multi-layer linear elastic (LE) model, using ALIZE-LCPC software. The elastic moduli of the UGM and subgrade layers were determined by backcalculation of FWD measurements made at the beginning of the experiment (see Table 4). Then for the elastic modulus of the asphalt layer, it was chosen to get the same asphalt peak strain ($A_{max}$) as the experimental one, for each section. It is interesting to note that this elastic stiffness modulus of the asphalt layer can be considered as an equivalent stiffness modulus at a frequency of 11.7 Hz corresponding to the traffic speed of 57 km/h (determined from the loading time of the strain signal as presented in section 3.1) and to an asphalt temperature of 18.4°C (measured during the tests). Following that consideration, such a modulus value represents an apparent stiffness modulus of the two asphalt layers together, in each studied pavement section at the considered testing condition (including a different interface condition).

- A second series of calculations was performed with the Viscoroute software (Chabot et al., 2010; Duhamel et al., 2005), which takes into account the linear viscoelastic (LVE) behavior of the asphalt layers, with a bonded interface. Viscoroute uses the Huet-Sayegh model, and the model parameters were determined from the complex modulus test performed on the asphalt mix used in situ (see section 2.1.2). For this reason, the same LVE properties were used for all three studied pavement sections as they were built with the same asphalt material. In this case, the model parameters could not be adjusted on the measured

maximum strains, which explains the larger difference of the modeling results with the experimental measurements. The LVE model is applicable to describe the response of the reference section, without a grid, but not for describing the "equivalent behavior" of sections with grids and variable interface conditions. For the UGM and subgrade layers, the same elastic moduli were used as for the LE calculations. These moduli were determined by backcalculation of FWD measurements made at the beginning of the experiment.

Table 4. Mechanical properties used for the modeling of the three studied pavement sections, for a speed of 57 km/h, a temperature of 18.4°C and a 65 kN load.

| Section | | A | | B | | C | |
|---|---|---|---|---|---|---|---|
| | | LE | LVE | LE | LVE | LE | LVE |
| AC | Modulus (MPa) | 9 720 (18.4°C, 11.7Hz) | $E^*_{AC}$ (18.4°C, 57km/h) | 7 120 (18.4°C, 12.1Hz) | $E^*_{AC}$ (18.4°C, 57km/h) | 5 900 (18.4°C, 11.5Hz) | $E^*_{AC}$ (18.4°C, 57km/h) |
| | h (cm) | 11.4 | | 10.3 | | 10.3 | |
| UGM | Modulus (MPa) | 187.5 | | 150.3 | | 163.5 | |
| | h (cm) | 30 | | | | | |
| Soil | Modulus (MPa) | 162.9 | | 155.7 | | 159.0 | |
| | h (cm) | 260 | | | | | |
| Concrete substratum | Modulus (MPa) | 55 000 | | | | | |

LE: linear elastic; LVE: linear viscoelastic; $E^*_{AC}$ from Table 1 ($|E^*|$ = 10 950 MPa at 18.4°C and 11.7 Hz).

Figure 9 presents comparisons between measured and calculated strains, for the three pavement sections. The results show that:

- In each of the three pavement sections, while experimental measurement and LE modeling of the strain signals lead to the same maximum tensile strains, LVE modeling gives a slightly lower maximum strain, because the modeling is carried out with laboratory determined parameters, and it is not possible to calibrate them on the in-situ measured strains. According to Table 4, the asphalt layer stiffness

moduli used in the LE models, for the reference sections A (without grid) and sections B (with 100 kN grid) and C (with 50 kN grid), were reduced respectively by 11.2%, 35.0%, and 46.1% compared to the ones used in the LVE model for the same temperature of 18.4°C and equivalent frequency of 11.7 Hz.

- Both LE and LVE models simulate well the shape of the experimental strain signals. However, some differences can be observed. Previous studies (Blanc et al., 2019) have shown that such differences can be due to the imperfect positioning of the strain gauges during their installation, to irreversible behavior of the asphalt layers, or to dynamic effects of the moving loads not considered in both models.

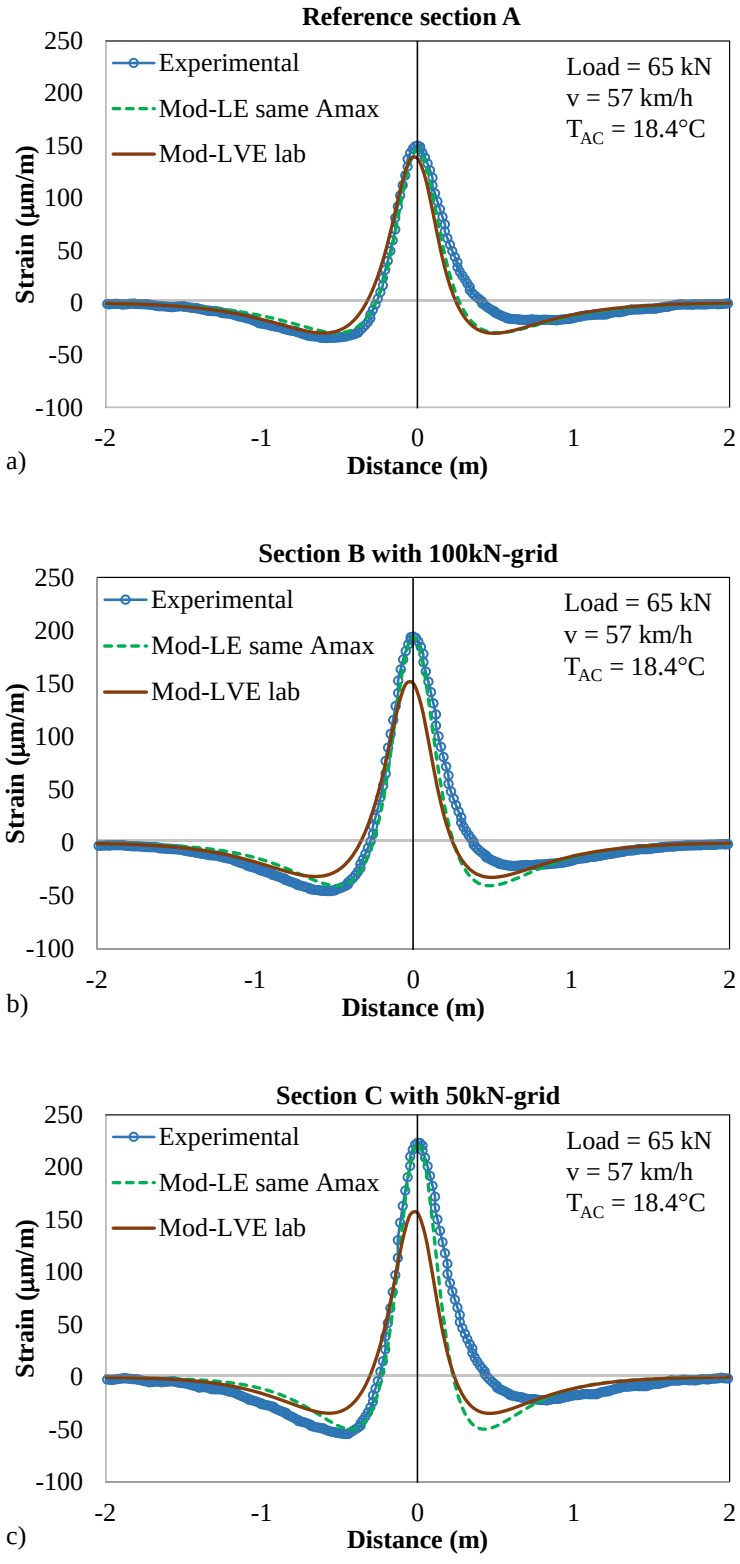


Figure 9. Comparison of measured strain signals and modeling (using linear elastic (LE) model with fitted in-situ measured maximum tensile strain or linear viscoelastic (LVE)

model with laboratory determined parameters), for strains at the bottom of the base asphalt layer at the same conditions in: a) Section A, b) Section B, c) Section C.

### *3.4. ASTSs procedure and temperature correction*

This procedure, which acronym stands for **A**sphalt layer **S**tiffness from measurements at different **T**raffic **S**peed**s** (ASTSs), is based on a combination of experimental measurements and numerical simulations presented in the previous sections. It can be synthesized as follow for the pavement structures in this study:

- For a given longitudinal strain signal obtained at each given traffic speed in a set of measurements at different speeds and a given recorded temperature in the asphalt layer, determining a numerical value of asphalt layer elastic stiffness ($E_{AL}$) that gives a calculated maximum tensile strain ($A_{max}$) matching the measured one. For that LE calculation, using Alizé-LCPC software, the stiffness moduli of the UGM ($E_{UGM}$) and soil ($E_{Soil}$) layers were taken from backcalculation of FWD measurement carried out close to the period of consideration.
- For the same strain measurement, the corresponding equivalent frequency can be determined directly from Equation (5).
- Repeat the above steps for the whole set of strain measurements at different speeds, to determine a set of asphalt layer stiffness moduli at the given recorded temperature.

Figure 10 illustrates the asphalt layer stiffness values determined from experimental data presented in Figure 7 by applying the ASTSs procedure, for a set of measurements at different traffic speeds (between 7 and 86 km/h), at an asphalt temperature of 18°C, and under the same load of 65 kN. It can be observed that all the

curves of layer stiffness moduli obtained using the ASTSs procedure are almost parallel to the master curve of complex modulus determined from a laboratory test on the same asphalt material for the same frequency range. This shows that the in-situ asphalt layer material presents the same frequency dependency as measured on laboratory samples. However, the in-situ and laboratory moduli present some differences. In reference section A (without an interlayer system), the moduli obtained for the in-situ asphalt layer are parallel and slightly lower (by 9.9% in average for the considered frequency range) than the ones measured in laboratory. Some scatter can be observed for measurements at the two highest traffic speeds, where the in situ moduli increased, probably due to less accurate strain measurements at these high speeds. In sections B (with 100kN-grid) and C (with 50kN-grid), the obtained in-situ stiffness moduli are lower than in laboratory by 38.7% and 47.6% respectively in average for the considered frequency range).

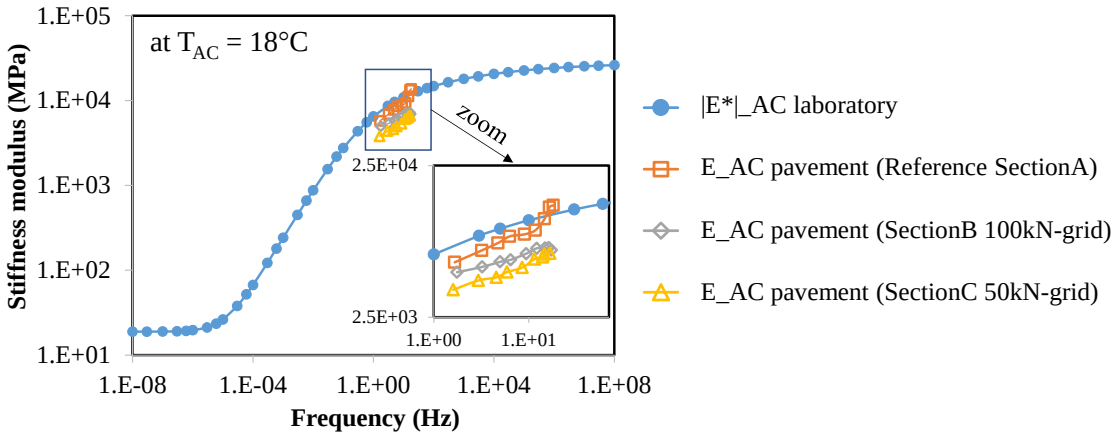


Figure 10. Comparison of stiffness moduli determined on asphalt pavement layers for the three studied sections at 18°C, using the ASTSs procedure, and master curve at the same temperature derived from laboratory moduli measured on material sample.

Based on these results, and with a first approximation, it is possible to estimate asphalt layer stiffness moduli for each of the studied pavement sections at another temperature ($T_i$) by translating first the laboratory master curve at 18°C (Figure 10) to

that temperature $T_i$, then subtracting the above corresponding differences. This approximation is considered as reasonable for the temperature range between 12 and 19°C registered during the different FWD campaigns (Table 3). This temperature correction procedure will be used in the following part of this paper. It is worth mentioning that it could be possible, by simplification, to apply directly the linear viscoelastic properties of the studied asphalt material measured in laboratory to perform a temperature correction for the stiffness moduli of the asphalt layer in the reference pavement section A. However, it can be seen in the results of the ASTSs procedure that it was not possible to do that for the two other sections B (with 100kN-grid) and C (with 50kN-grid) with different interface conditions because of higher differences between laboratory and in-situ moduli values (Figure 10).

## 4. Pavement behavior during the fatigue loading period

In this section, the evolution of the behavior of the three experimental pavements with traffic cycles is analyzed, based on data obtained from three monitoring methods. First, pavement damage evolution is analyzed based on asphalt strains and pavement surface cracking. Then, the focus is made on the evolution of the asphalt layer stiffness, by introducing a damage parameter, which can be used as a global indicator of the fatigue damage of the asphalt layers of the studied pavement structures.

### *4.1. Evolution of strain responses with load cycles*

This part presents the analysis of the strain response of the three pavement subsections with instrumentation (A1, B1, and C1), under 65 kN load level, during the APT experiment, up to 1.5 million cycles. Figure 11 presents the longitudinal strain signals measured at the bottom of the base layers for all three pavement sections, at several different numbers of cycles. Similarly, Figure 12 presents the strain signals measured at

the bottom of the surface layer, but only for sections A1 and B1, because the surface layer was not instrumented in section C1. The temperatures recorded in the asphalt layers at the same time are also plotted on these figures. These figures show that:

- The longitudinal strain signals presented increasing amplitudes, but their general shape remained the same from the beginning to the end of the test. That means there was no severe local damage (cracking or delamination) of the pavement layers at the position of these gauges (Nguyen et al., 2020b). Only the strain gauge EpsL located in the surface layer in section B (Figure 12b) ceased working after 1.5 million cycles. This could indicate a local damage at the position of this gauge.
- Regarding the longitudinal strains at the bottom of the base asphalt layer (Figure 11), it can be seen that they increased gradually throughout the loading period, even though the asphalt temperatures decreased slightly. This attests the development of fatigue damage in the pavement structures. In addition, it is interesting to note that strains increased much more in sections B1 and C1 (with interlayer systems) than in section A1 (without interlayer), indicating higher damage in sections B1 and C1.
- Regarding the longitudinal strains at the bottom of the surface asphalt layer (Figure 12), a similar gradual increase with traffic cycles can be observed in both sections A1 (reference) and B1 (with 100kN-grid). This strain evolution in the upper layer can probably be explained by a change in the bonding condition at the interface between the two asphalt layers, associated with the fatigue damage. However, it can be seen that the strain increase is lower in section B, which could be due to the reinforcement effect of the grid. It could also be due to a higher fatigue damage in the base layer in section B1 than in section A1 as discussed

above, which could have moved the neutral axis of the two asphalt layers in section B1 upwards, in comparison with section A1.

According to the above analysis, in these two-layer pavements, it seems that the variations of the magnitude of the asphalt strains with traffic are not only due to damage, but also to asphalt layer interface condition, and subsequent strain redistribution. Without a controlled damage using an artificial defect and dedicated instrumentation on both sides of that defect (similar to the work in Nguyen et al., 2020b), it is difficult to determine the influence of each of these mechanisms (fatigue cracking or interface debonding) on the measured strains. For that same APT experiment, in a recent work (Chupin et al., 2020), numerical simulations using a specific layer-wise approach were carried out for different damage scenarios to infer the (unknown) pattern of cracking/debonding development. However, further detailed destructive investigations (coring, or cutting of trenches) will need to be done for verification of the best modeled pattern scenario. In the present work, an alternative approach, based on asphalt layer stiffness evaluation, is presented and applied in the following section for determining the overall fatigue damage of the pavement.

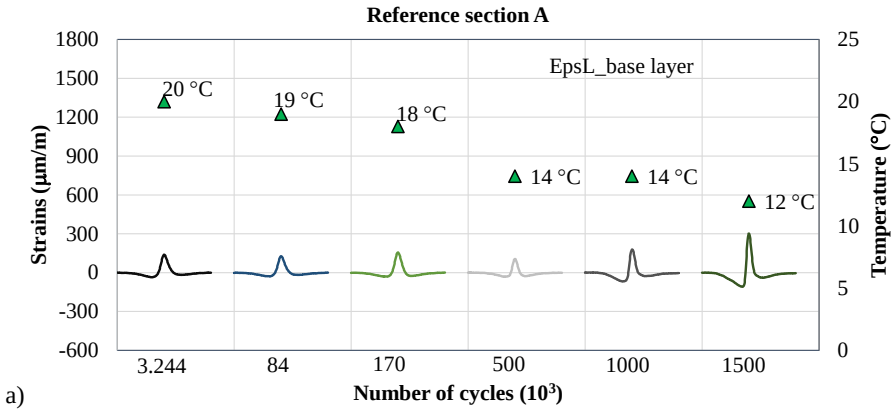


a)

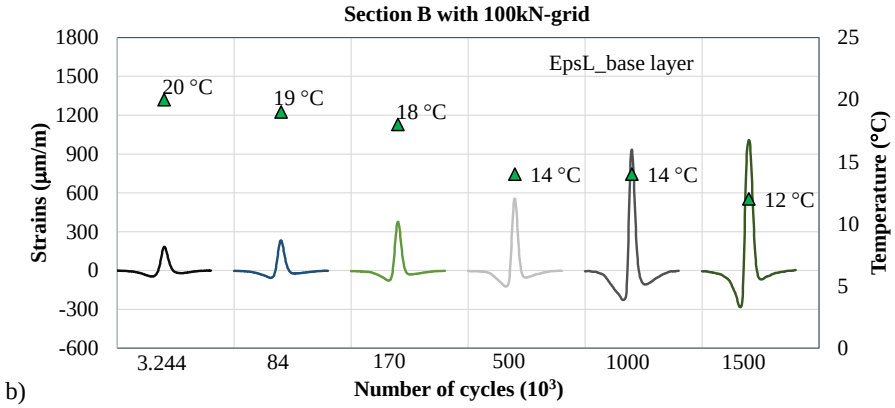


b)

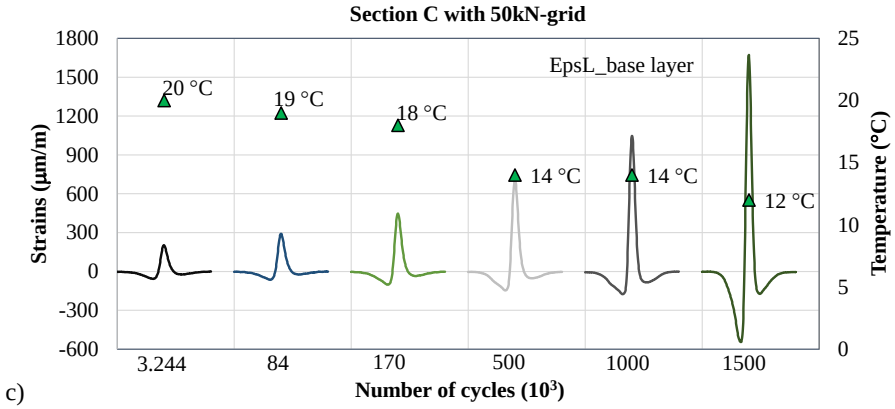


c)

Figure 11. Strain signals at the bottom of the base asphalt layer versus number of load cycles (for load level of 65 kN, and speed of 57 km/h) in the three pavement sections A (a), B (b) and C (c).

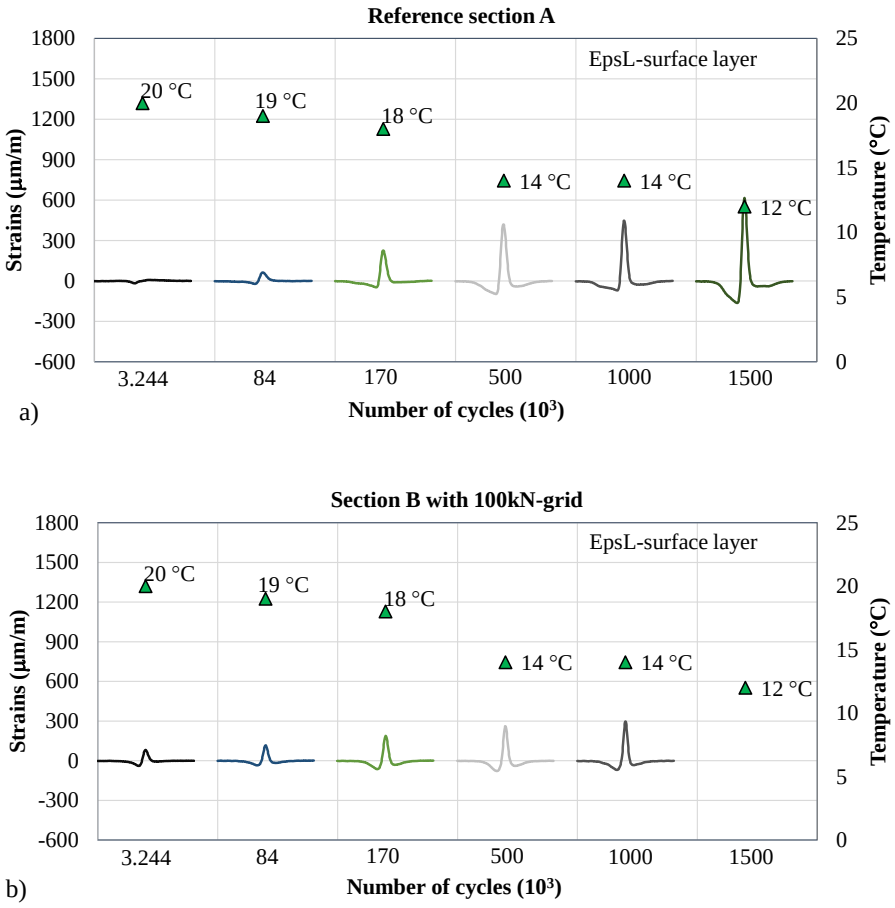


Figure 12. Strain signals at the bottom of the surface asphalt layer versus number of load cycles (for load level of 65 kN, and speed of 57 km/h) in the two pavement sections A (a) and B (b).

### *4.2. Pavement cracking evolution*

Figure 14 presents an example of maps of surface cracking of the three tested pavement sections, obtained at the end of the experiment. These crack maps show that, for each pavement section, the zones without instrumentation (n°2) present less cracking than the zones which have been instrumented using asphalt strain gauges (n°1). Although asphalt strain gauges are very useful for evaluation of mechanical behavior of pavements, it seems that in some cases, they can create defects in the pavement layer, and initiate cracking or other deteriorations (Nguyen et al., 2020a), especially when they are installed at a low depth below the pavement surface, as is the case in this experiment.

For this reason, on the APT facility of Université Gustave Eiffel, since about ten years, when it is possible, pavement sections are not instrumented over their entire length, in order to leave “control zones” without instrumentation. The crack maps also show that the instrumented sections with grids at the asphalt layers interface (B1 and C1) present more cracking than the reference section without a grid (A1). Differences in levels of cracking are less visible on the sub-sections without instrumentation: no crack is visible on reference sub-section A2; sub-section C2 (with 50kN-grid) has two visible cracks near its end, close to the joint; sub-section B2 (with 100kN-grid) has more cracks, distributed along the section length.

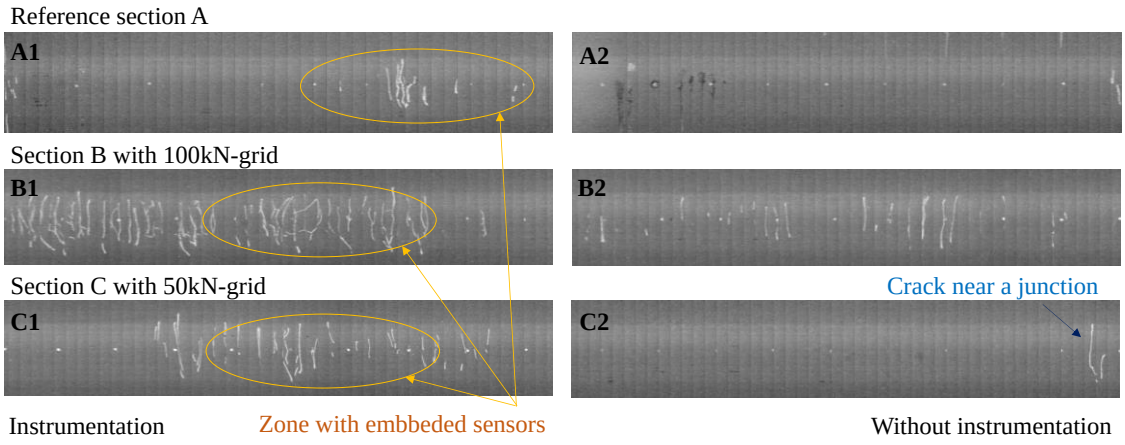


Figure 13. Surface crack maps of the tested pavement sections, after 2.2 million load cycles.

The crack evolutions on each pavement section, expressed in terms of percentage of cracking, corresponding to the ratio between the pavement section length affected by visible cracks and its total length, are plotted in Figure 14, as a function of the number of load cycles. These crack evolutions will be used to compare with a damage ratio proposed in the following section.

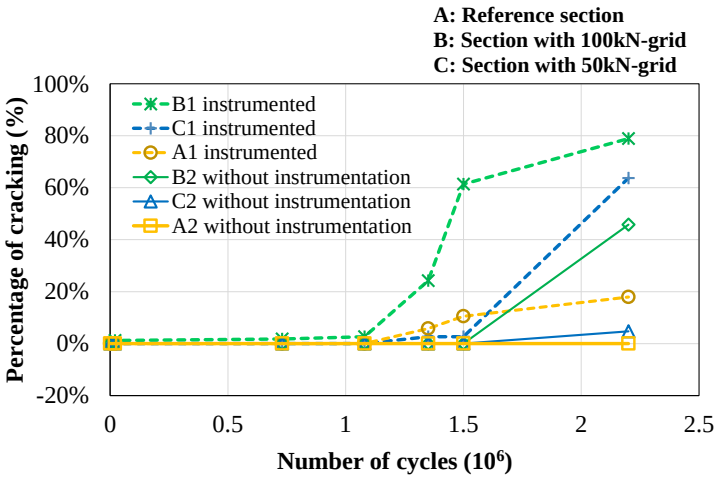


Figure 14. Evolution of the percentage of cracking with traffic loading observed on the tested pavement sections.

### *4.3. Evolution of asphalt layer stiffness with load cycles*

Aging, post compaction, and fatigue damage have been known as the most important factors affecting the stiffness of asphalt layers during the pavement service life (Mateos et al., 2012; Yin et al., 2017). Aging and post compaction mostly take place during the beginning of the service life, and lead to an increase of the asphalt layer stiffness. On the other hand, fatigue damage develops continuously with cumulative traffic, along with the pavement service life, and tends to decrease the asphalt layer stiffness.

Using FWD measurements is an effective way to evaluate, by backcalculation, the pavement layer stiffness moduli, especially for asphalt layers. Figure 15 presents the evolution of backcalculated asphalt layer moduli with the number of load cycles, for the three studied pavement sections, distinguishing subsections with and without instrumentation. The curves clearly present two parts: during the first part, up to about 500 000 to 700 000 load cycles, the moduli remain stable, or even increase, due probably to post-compaction of the asphalt layers. Then, after this first phase, the moduli start to decrease, indicating the development of damage. The decrease is more important, in all

cases, for the instrumented subsections, due probably to the defects created by the strain gauges.

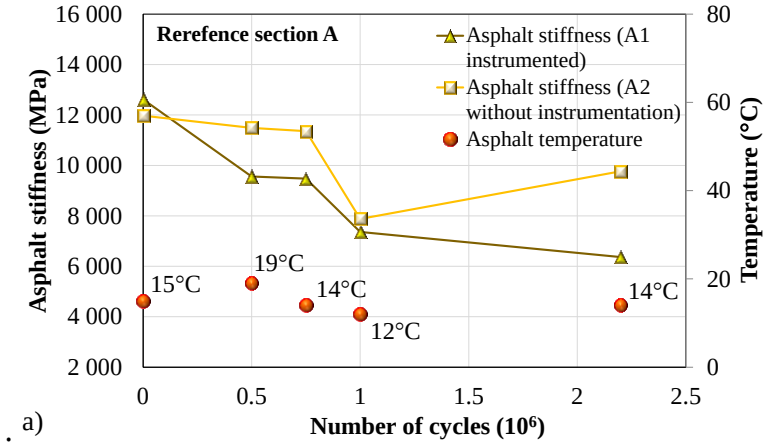


a)

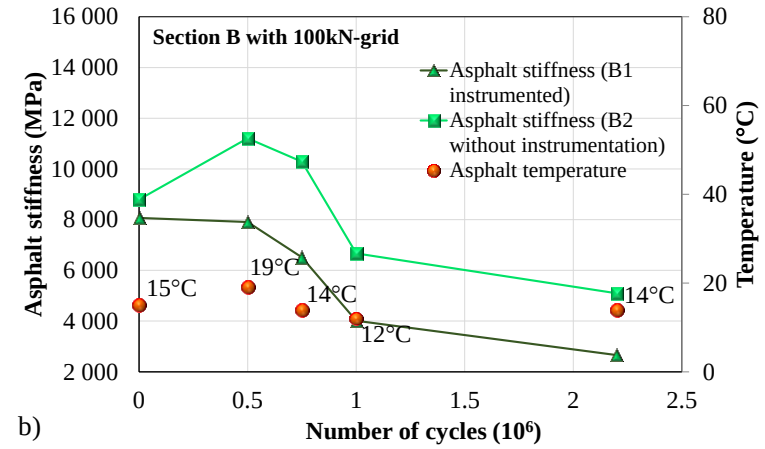


b)

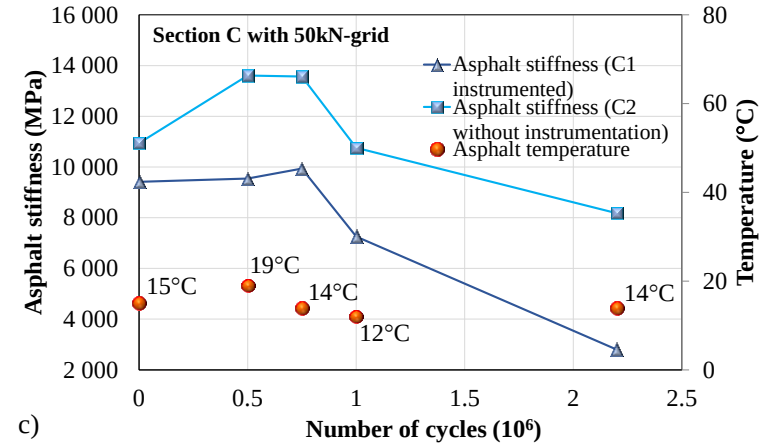


c)

Figure 15. Evolution of asphalt layer stiffness versus number of load cycles in:
a) reference section A; b) section B with 100kN-grid; c) section C with 50kN-grid.

However, a direct comparison of the asphalt layer moduli obtained at different numbers of load cycles is not straightforward, due to temperature differences between the different FWD campaigns (see Table 3). Therefore for each section, a stiffness modulus-based damage ratio, noted $D_E^T$ (Equation (6)), has been introduced. It describes the relative evolution with the number of load cycles of the asphalt layer stiffness ($E_{Ni}^{Ti}$) at cycle i ($N_i$) and at a given asphalt temperature $T_i$ (registered in each corresponding FWD campaign), with reference to the initial value ($E_{N0}^{Ti}$) before the application of traffic (i.e. at cycle 0) and at the same temperature. For that, the temperature correction procedure presented at the end of section 3.4 was applied to determine those stiffness values ($E_{N0}^{Ti}$).

$$D_E^{Ti} = 1 - \frac{E_{Ni}^{Ti}}{E_{N0}^{Ti}} \quad (6)$$

where:

$D_E^{Ti}$: stiffness modulus-based damage ratio at temperature $T_i$;

$E_{N0}^{Ti}$: asphalt layer stiffness modulus at cycle zero ($N_0$) and temperature $T_i$, determined by application of the temperature correction procedure (presented in section 3.4);

$E_{Ni}^{Ti}$: asphalt layer stiffness modulus at cycle i$^{th}$ ($N_i$) of each FWD campaign, determined by backcalculation from FWD measurements made at cycle i and at temperature $T_i$.

Using Equation (6), it was possible to calculate a damage ratio for each number of load cycles, corresponding to each FWD campaign. Finally, to be able to analyze the evolution of these damage ratios with the number of load cycles, it was assumed that this evolution is independent of temperature. This assumption can be considered as reasonable, at least for the limited range of temperatures at which the different FWD campaigns were made (between 12 and 19°C).

The evolution of the damage ratios $D_E^T$ for the three experimental pavement sections are plotted in Figure 16, and compared with the surface cracking (presented in section 4.2). For the reference pavement section, the results are also compared with the level of fatigue damage predicted by the French mechanistic pavement design method (NF P98-086, 2019), which is only applicable to the unreinforced section. These figures show that:

- "Negative" damage ratios, indicating a stiffness increase, are obtained on all sections except subsection A1 (reference section with instrumentation), between 0 and about 750 000 cycles. This can be attributed to post compaction and aging of the asphalt layers, which occurred at the beginning of the experiment.
- This stiffness increase is less important in the sections without a grid or with instrumentation.
- Figure 16a also shows that the measured evolution of the damage ratio in subsection A1 (reference section with instrumentation) is in good agreement with the damage level predicted by the French pavement design method.
- The comparison of the evolution of surface cracking with the asphalt layer damage ratio in each section first confirms the observation that pavement damage started to develop before the first cracks appeared on the pavement surface. This comparison shows that cracking started to appear on the pavement surface at a threshold of about 50% of asphalt layer damage, for all the sections with instrumentation (reference section A1, B1 with 100kN-grid, and C1 with 50kN-grid). This appearance of surface cracking at a damage level of 50 % is in agreement with assumptions made in France for the calibration of the pavement design method, for the fatigue criterion. However, the levels of damage corresponding to the first surface cracks in sections B2 (with 100kN-grid) and C2

(with 50kN-grid) are lower, respectively 37% and 18%. This result means that these sub-sections without instrumentation and with a different type of grid had different (lower) thresholds of damage for the onset of surface cracking. Sub-section A2 (reference) had a similar damage level at the end of the APT experiment at 2.2 million cycles (higher at 1 million cycles) as sub-section C2 (with 50kN-grid) even though the latter had a lower asphalt thickness (1.1 cm less) than the reference section.

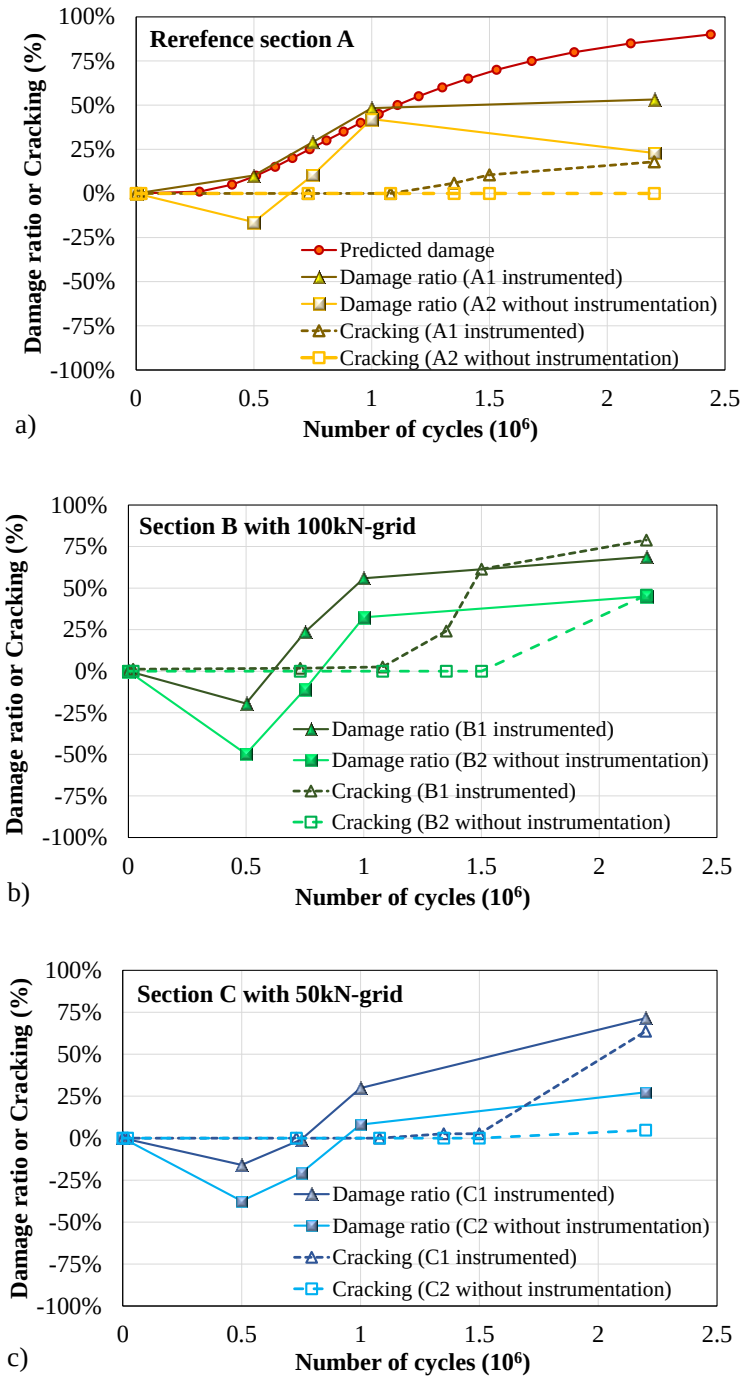


Figure 16. Evolution of damage ratio and pavement surface cracking versus number of load cycles in: a) the reference section A (with pavement damage predicted by the French design method); b) section B with 100kN-grid; c) section C with 50kN-grid.

## 5. Conclusions and perspectives

This study investigated the mechanical behavior of pavement structures with two asphalt layers with or without an interlayer system at the interface, from the beginning to the end

of an APT experiment. This analysis on such studied pavement structures having different interface conditions was made possible thanks to the proposal of an original ASTSs procedure. Both the linear viscoelastic response in non-damaged condition and the evolution of damage with load cycles of the asphalt layers were studied based on the association of different monitoring methods. Based on the results discussed in the paper, the following conclusions can be drawn:

- In non-damaged condition:
    - Maximum tensile strains in the asphalt layer decrease with increasing loading speeds, following a negative exponential function in the measurement range. For a larger frequency domain, they might follow a negative sigmoidal function.
    - Equivalent loading frequencies for modeling of pavement response can be determined based on the loading times of strain signals. They vary linearly with the loading speed. The slope of this relationship increases with the asphalt layer temperature, but is not affected by the load level.
    - The proposed original ASTSs procedure can be used to estimate the asphalt layer stiffness, from measurements made at different traffic speeds, without knowing the linear viscoelastic properties of the asphalt material. Such procedure allows determining an isotherm curve (i.e. at a constant temperature) of the asphalt layer stiffness modulus, over the investigated equivalent loading frequency range. However, it requires knowing the stiffness moduli of the other pavement layers, which can be determined for instance via backcalculation of FWD measurements. This

approach can be extended to measurements at different temperatures, to determine a larger range of equivalent stiffness moduli of the asphalt layer.

- During the fatigue loading period:
    - Asphalt strain response evolved with applied traffic. However, these local measurements are not suitable for estimating an "average" asphalt layer damage. The strain gauge response is very dependent on local crack development, and on interface bonding conditions, which lead to a redistribution of strains in the pavement structure.
    - The proposed approach for the determination of a stiffness modulus-based damage ratio seems more appropriate to evaluate pavement damage during an APT full-scale fatigue experiment. It allowed monitoring the relative evolution of the asphalt layer stiffness with the number of load cycles with reference to its initial value in each of the studied pavement sections from the beginning, even before the onset of surface cracking, to damaged condition.
    - The proposed approach enabled to compare the damage evolution between different studied pavement sections. Among them, sub-section C2 without instrumentation and with the 50kN-grid at the asphalt layer interface presented the lowest damage evolution.

**Acknowledgments**

Part of the experimental data used in this study came from the full-scale test sponsored by the French National Research Agency (ANR-SolDuGri project ANR-14-CE22-0019).

## Disclosure statement

No potential conflict of interest was reported by the author(s).

## References


Austroads, (2012). Guide to Pavement Technology-Part 2: Pavement Structural Design, 3rd ed., Austroads, Sydney, Australia.

Autret, P., De-boissoudy, A.B., & Gramsammer, J.C. (1987). The circular test track of the Laboratoire Central des Ponts et Chaussées – First Results. *Proceedings of 6th International Conference on Structure Design of Asphalt Pavements*, *1*, 550–561.

Bari, J., & Witczak, M. W. (2006). Development of a new revised version of the Witczak E Predictive Model for hot mix asphalt mixtures. *Proceedings of the Technical Sessions of the Conference Asphalt Paving Technology: Association of Asphalt Paving Technologists*, *75*, 381–424.

Barksdale, R. D. (1971). Compressive stress pulse times in flexible pavements for use in dynamic testing. *Highway Research Record*, *345*. https://trid.trb.org/view/104721

Blanc, J., Hornych, P., Sotoodeh-Nia, Z., Williams, C., Porot, L., Pouget, S., Boysen, R., Planche, J.-P., Lo Presti, D., Jimenez, A., & Chailleux, E. (2019). Full-scale validation of bio-recycled asphalt mixtures for road pavements. *Journal of Cleaner Production*, *227*, 1068–1078. https://doi.org/10.1016/j.jclepro.2019.04.273

Bodin, D., Chupin, O., & Denneman, E. (2017). Viscoelastic Asphalt Pavement Simulations and Simplified Elastic Pavement Models Based on an "Equivalent Asphalt Modulus" Concept. *Journal of Testing and Evaluation*, *45*(6), 20160652. https://doi.org/10.1520/JTE20160652

Brown, S. F. (1973). Determination of Young's modulus for bituminous materials in pavement design. *Highway Research Record, 431*. https://trid.trb.org/view/125575

Burmister, D. M. (1943). The theory of stress and displacements in layered systems and applications of the design of airport runways. *In: Proceedings of the Highway Research Board*, *23*.

Chabot, A., Chupin, O., Deloffre, L., & Duhamel, D. (2010). ViscoRoute 2.0 A: Tool for the Simulation of Moving Load Effects on Asphalt Pavement. *Road Materials and Pavement Design*, *11*(2), 227–250. https://doi.org/10.1080/14680629.2010.9690274

Chailleux, E., Ramond, G., Such, C., & de La Roche, C. (2006). A mathematical-based master-curve construction method applied to complex modulus of bituminous materials. *Road Materials and Pavement Design*, *7*(sup1), 75–92. https://doi.org/10.1080/14680629.2006.9690059

Chupin, O., Piau, JM., Chabot, A., Nasser, H., Nguyen, M.L., Lefeuvre, Y. (2020). Simulation of Damage Scenarios in a Bituminous Pavement Tested Under FABAC ALT Using M4-5n. In: Chabot, A., Hornych, P., Harvey, J., Loria-Salazar, L. (Eds), *Accelerated Pavement Testing to Transport Infrastructure Innovation*. Lecture Notes in Civil Engineering, vol 96. Springer. https://doi.org/10.1007/978-3-030-55236-7_40

Duhamel, D., Chabot, A., Tamagny, P., & HARFOUCHE, L. (2005). Viscoroute: Visco-elastic modeling for asphalt pavements - Viscoroute : Modélisation des chaussées bitumineuses. *Bulletin Des Laboratories Des Ponts et Chaussees*, 89–103.

EN 12591. (2009). *Bitumen and bituminous binders—Specifications for paving grade bitumens*. European Standard Norm.

EN 12697-26. (2018). *Bituminous Mixtures—Test Methods for Hot Mix Asphalt—Part 26: Stiffness*. European Standard Norm.

EN 13808. (2013). *Bitumen and bituminous binders—Framework for specifying cationic bituminous emulsions*. European Standard Norm.

Francken, L. (1997). *Prado: Logiciel de calcul.* Centre de Recherche Routière (CRR), Bruxelles.

Godard, E., Chazallon, C., Hornych, P., Nguyen, M. L., Doligez, D., Pelletier, H., Michel, D., Laurence, L., & Brissaud, L. (2019). Projet Soldugri – Avancement de l'étude du renforcement des enrobés bitumineux par de grilles de verre. RGRA, 967.

Hornych, P., Kerzreho, J. P., Chabot, A., Bodin, D., Balay, J. M., & Deloffre L. (2008). In Pavement Cracking - Al-Qadi, Scarpas & Loizos (eds). *The LCPC's ALT facility contribution to pavement cracking knowledge*. https://doi.org/10.13140/2.1.2361.9529

Huet, C. (1963). *Etude par une méthode d'impédance du comportement viscoélastiques des matériaux hydrocarbonnées (PhD thesis).* Université de Paris.

Le, X. Q., Nguyen, M. L., Hornych, P., Nguyen, Q. T., Godard, E., Legal, Y., Brissaud, L., Doligez, D., Chazallon, C. (2022). Evaluation of interface bonding condition on mechanical responses of full-scale asphalt pavements with and without grid reinforcement. *Accepted to BCRRA 2022*, Trondheim, Norway.

Marasteanu, M. O., & Anderson, D. A. (1999). Improved Model for Bitumen Rheological Characterization. *Eurobitume Workshop on Performance Related Properties for Bituminous Binders, 133*.

Mateos, A., Ayuso, J. P., & Jáuregui, B. C. (2012). Evolution of Asphalt Mixture Stiffness under Combined Effects of Damage, Aging, and Densification under Traffic. *Transportation Research Record: Journal of the Transportation Research Board*, *2304*(1), 185–194. https://doi.org/10.3141/2304-21

Mshali, M. R. S., & Steyn, W. JvdM. (2020). Effect of truck speed on the response of flexible pavement systems to traffic loading. *International Journal of Pavement Engineering*, 1–13. https://doi.org/10.1080/10298436.2020.1797733

NF EN 13108–1. (2007). *Bituminous mixtures—Material specifications—Part 1: Bituminous mixes, in French*. Association Française de Normalisation (AFNOR).

NF P98-086. (2019). *Dimensionnement structurel des chaussées routières—Application aux chaussées neuves*. Association Française de Normalisation (AFNOR).

Nguyen, M. L., Blanc, J., Trichet, S., Gouy, T., Coirier, G., Baudru, Y., Le, X. Q., Nguyen, M. D., Siroma, R. S., Hornych, P., & Blaineau, F. (2020a). Rapid and Continuous Imaging for Crack Monitoring During APT Experiments. In A. Chabot, P. Hornych, J. Harvey, & L. G. Loria-Salazar (Eds.), *Accelerated Pavement Testing to Transport Infrastructure Innovation*. Lecture Notes in Civil Engineering, vol. 96 (pp. 649–657). Springer. https://doi.org/10.1007/978-3-030-55236-7_67

Nguyen, M. L., Chupin, O., Blanc, J., Piau, J.-M., Hornych, P., & Lefeuvre, Y. (2020b). Investigation of Crack Propagation in Asphalt Pavement Based on APT Result and LEFM Analysis. *Journal of Testing and Evaluation*, *48*(1), 20180933. https://doi.org/10.1520/JTE20180933

Olard, F., & Di Benedetto, H. (2003). General "2S2P1D" Model and Relation Between the Linear Viscoelastic Behaviors of Bituminous Binders and Mixes. *Road*

*Materials and Pavement Design*, *4*(2), 185–224. https://doi.org/10.1080/14680629.2003.9689946

Sayegh, G. (1967). *Contribution à l'étude des propriétés viscoélastiques des bitumes purs et des bétons bitumineux (PhD thesis).* Université de Paris.

Swett, L., Mallick, R. B., & Humphrey, D. N. (2008). A study of temperature and traffic load related response in different layers in an instrumented flexible pavement. *International Journal of Pavement Engineering*, *9*(5), 303–316. https://doi.org/10.1080/10298430701576117

Timm, D. H., & Priest, A. L. (2008). Flexible pavement fatigue cracking and measured strain response at the NCAT test track. *Transportation Research Board 87th Annual Meeting*.

Ulloa, A., Hajj, E. Y., Siddharthan, R. V., & Sebaaly, P. E. (2013). Equivalent Loading Frequencies for Dynamic Analysis of Asphalt Pavements. *Journal of Materials in Civil Engineering*, *25*(9), 1162–1170. https://doi.org/10.1061/(ASCE)MT.1943-5533.0000662

Willis, R., Timm, D., West, R., Powell, B., Robbins, M., Taylor, A., Smit, A., Tran, N., Heitzman, M., & Bianchini, A. (2009). *Phase III NCAT Test Track Findings* (NCAT 09-08; p. 137). National Center for Asphalt Technology, Auburn University.

Yin, F., Arámbula-Mercado, E., Epps Martin, A., Newcomb, D., & Tran, N. (2017). Long-term ageing of asphalt mixtures. *Road Materials and Pavement Design*, *18*(sup1), 2–27. https://doi.org/10.1080/14680629.2016.1266739